

## Article

# Effect of Ta Content on Microstructure and Properties of (Ti,W)C-Based Cermets

Song Zhang<sup>1</sup>, Junfeng Liao<sup>1</sup>, Meijun Yang<sup>1</sup>, Baifeng Ji<sup>2</sup> , Qizhong Li<sup>1,3,\*</sup>, Takashi Goto<sup>1,4</sup> and Rong Tu<sup>1,5</sup> 

- <sup>1</sup> Chaozhou Branch of Chemistry and Chemical Engineering Guangdong Laboratory, State Key Laboratory of Advanced Technology for Materials Synthesis and Processing, Wuhan University of Technology, 122 Luoshi Road, Wuhan 430070, China; kobe@whut.edu.cn (S.Z.); 15005543290@163.com (J.L.); liyangmeijun@163.com (M.Y.); goto@imr.tohoku.ac.jp (T.G.); turong@whut.edu.cn (R.T.)
- <sup>2</sup> School of Civil Engineering and Architecture, Wuhan University of Technology, Wuhan 430070, China; jbfeng@whut.edu.cn
- <sup>3</sup> Hubei Key Laboratory of Advanced Technology for Automotive Components, Wuhan University of Technology, Wuhan 430070, China
- <sup>4</sup> New Industry Creation Hatchery Center, Tohoku University, Sendai 980-8577, Japan
- <sup>5</sup> Wuhan University of Technology Advanced Engineering Technology Research Institute of Zhongshan City, Xiangxing Road 6, Zhongshan 528400, China
- \* Correspondence: qizhongli@whut.edu.cn; Tel.: +86-13437161925

**Abstract:** (Ti,W)C-based cermets are an ideal material for the preparation of high-performance cutting tools due to their excellent mechanical properties, high temperature oxidation resistance, and corrosion resistance. However, their lower toughness limits the application of cutting tools. In order to solve the problem of low toughness faced by the current materials used in tools, in this study, a (Ti,W)C solid solution was used as the hard phase to prepare cermets with high toughness via vacuum sintering. The effects of Ta content on the composition, morphology, and microstructure of the cermets were analyzed through XRD analysis and SEM and EDS characterization methods. The mechanical properties such as hardness, transverse fracture strength, and the fracture toughness of the cermets and corrosion resistance in an HNO<sub>3</sub> solution were also investigated. The results show that the microstructure of (Ti,W)C solid solution-based cermets exhibit simpler core-rim (single-rim) and acyclic structures, which weaken the formation and propagation of cracks at the interface. The relative density and grain size of cermets increases and decreases, respectively, with the greater amount of Ta addition, while excessive Ta addition leads to a decrease in the relative density and agglomeration between grains. The cermet with 3 wt.% Ta addition possessed excellent mechanical properties with a Vickers hardness, transverse rupture strength, and fracture toughness of 13 GPa, 1907.4 MPa, and 15.5 MPa m<sup>1/2</sup>, respectively. The addition of Ta leads to the formation of a Ta-rich protective layer on the surface of the cermet under the corrosion of the acidic solution, and with the increase in the Ta content, the corrosion resistance of the cermet gradually improves.

**Keywords:** (Ti,W)C solid solution; cermet; microstructure; mechanical properties; corrosion resistant



**Citation:** Zhang, S.; Liao, J.; Yang, M.; Ji, B.; Li, Q.; Goto, T.; Tu, R. Effect of Ta Content on Microstructure and Properties of (Ti,W)C-Based Cermets. *Metals* **2022**, *12*, 1282. <https://doi.org/10.3390/met12081282>

Academic Editors: Haiming Ding, Peng Wang and Xiangguang Kong

Received: 11 July 2022  
Accepted: 26 July 2022  
Published: 29 July 2022

**Publisher's Note:** MDPI stays neutral with regard to jurisdictional claims in published maps and institutional affiliations.



**Copyright:** © 2022 by the authors. Licensee MDPI, Basel, Switzerland. This article is an open access article distributed under the terms and conditions of the Creative Commons Attribution (CC BY) license (<https://creativecommons.org/licenses/by/4.0/>).

## 1. Introduction

Traditional WC-Co cemented carbides are widely used in the tool industry; however, their low high-temperature hardness, chemical stability, oxidation resistance, and corrosion resistance limit their applications in high-speed cutting and other fields [1]. TiC- and Ti(C,N)-based cermets are new cermet materials with excellent hardness, perfect thermal impact resistance, superior wear resistance, high corrosion resistance, and good chemical stability. Due to their excellent comprehensive mechanical properties, TiC- and Ti(C,N)-based cermets are used as effective alternatives to WC-Co in cutting tools [2,3]. In general, cermets consist of two distinct phases: the ceramic phase and the metal binder phase. The ceramic parts retain high hardness and cutting ability, whereas the soft binder

encounters deformation and absorption energy [4–7]. However, the Ti(C,N)-based cermets exhibit lower toughness than traditional WC–Co cemented carbides, thereby limiting their applications as a type of cutting-tool material [8].

In order to improve the toughness of Ti(C,N) cermets, secondary carbides such as WC are introduced into TiC–Ni and Ti(C,N)–Ni cermets. The typical core–rim structure is formed upon the addition of secondary carbides. The core phase consists of dissolved ceramic particles, and the rim phase is formed by a dissolution–precipitation mechanism during the liquid phase sintering stage [9,10]. Different from the two-phase structure of WC–Co carbide, the microstructure of TiC- and Ti(C,N)-based cermets with an added secondary carbide have a complex multiphase structure, due to the different phases with different physical properties, resulting in the increase of the microstructure of the interface stress and easier crack formation and propagation at the interface. The results have shown that two or more kinds of carbide materials can be prepared into solid solution materials by pre-solution treatment, and the two-phase-structured cement similar to WC–Co cemented carbide can be prepared using solid solution materials as a hard phase [11,12]. In view of this, (Ti,W)C–Ni-based cermets with (Ti,W)C solid solution powder as a hard phase were expected to obtain better properties.

The contact angle between the solid solution of  $(\text{Ti}_{0.77}\text{W}_{0.23})\text{C}$  and Ni is only  $16^\circ$  when the temperature is  $1420^\circ\text{C}$  in a vacuum environment, which does not lead to complete wetting [13]. Therefore, in the preparation of (Ti,W)C–Ni-based cermets with the (Ti,W)C solid solution, an appropriate amount of Mo is typically added to improve the wettability between the hard phase and the metal binder phase [14]. Kieffer et al. reported that N affects the dissolution of various elements in the system, which can effectively inhibit the growth of the annular phase, thus refining the grain and improving the comprehensive mechanical properties of cermets, especially the redness, strength and toughness, and resistance to plastic deformation [15]. Previous studies have shown that an intergranular fracture (along the grain boundaries) is usually the main failure mode of cermets [16]. The introduction of TiN as the N source into the TiC cermet can limit crack propagation and improve the toughness of the material. Studies have shown that the presence of WC improves the corrosion rate of materials and reduces their corrosion resistance. Further, the addition of Ta is conducive to the improvement in the corrosion resistance of materials in acidic solutions [17]. In addition, studies have shown that the addition of Ta or TaC to TiC and Ti(C,N) cermets can improve the wettability between the hard phase and the metal binder phase. In the sintering process, Ta and the TiC or Ti(C,N) cermet form a solid solution to change the core ring structure and reduce the interface energy of the system. Further, the addition of Ta can inhibit grain growth, enhance the mechanical properties of materials, and enhance the cutting performance of tools [18]. However, the addition of excess Ta will reduce the density and performance of the material. In this regard, the effects of Ta or TaC on the microstructure, mechanical properties, and corrosion resistance of (Ti,W)C–Ni-based cermets have rarely been studied.

In this study, the (Ti,W)C solid solution powder was used as the hard phase and Ni was used as the metal binder phase to prepare the two-phase-structured cermet. The effect of the Ta content on the microstructure, mechanical properties, and corrosion resistance of (Ti,W)C–Ni-based cermets was thoroughly studied.

## 2. Materials and Methods

Commercial powder raw materials used in this study include (Ti,W)C, Ni, Ta, Mo, TiN,  $\text{Cr}_3\text{C}_2$ , and C with average particle sizes of  $1\text{--}3\ \mu\text{m}$ ,  $1\text{--}3\ \mu\text{m}$ ,  $1\text{--}3\ \mu\text{m}$ ,  $1\text{--}3\ \mu\text{m}$ ,  $1\text{--}10\ \mu\text{m}$ ,  $10\text{--}30\ \mu\text{m}$ , and  $10\text{--}20\ \mu\text{m}$ , respectively. Figure 1 displays the SEM images of (Ti,W)C and mixed powders. Tables 1 and 2 show the chemical composition of (Ti,W)C solid solution powder and the raw material ratio of the cermet. Graphite powder (1 wt.%) and  $\text{Cr}_3\text{C}_2$  were used as the deoxidiser for strengthening the solution and for grain growth inhibition, respectively.

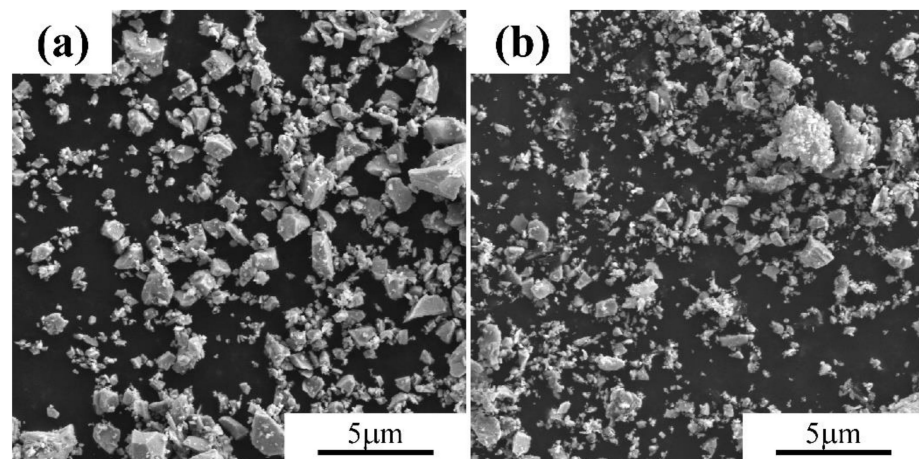


Figure 1. SEM images of powders: (a) (Ti,W)C powders, (b) (Ti,W)C-3Ta mixed powders.

Table 1. Chemical composition of (Ti,W) C solid solution powders (wt.%).

Cermet	Components (wt.%)			
	Ti	W	C	Impurities
(Ti,W)C	40.07	46.86	12.6	Balance

Table 2. Composition of raw material powder (wt.%).

Cermet	Components (wt.%)						
	(Ti,W)C	TiN	Ni	Mo	C	Cr <sub>3</sub> C <sub>2</sub>	Ta
A	46	10	30	12	1	1	0
B	45	10	30	12	1	1	1
C	43	10	30	12	1	1	3
D	41	10	30	12	1	1	5

The XGB4-type omnidirectional planetary ball mill was used for mixing. The grinding ball material consisted of WC-Co carbide balls and the ball-to-material ratio was 7:1. A certain proportion of anhydrous ethanol was poured for wet grinding, the speed was set to 250 r/min, and the ball-milling time was 48 h. After ball milling and mixing, the slurry was placed in a DZF-6050/4 electric heating vacuum drying oven and dried at 80 °C for 8 h to ensure complete removal of anhydrous ethanol. The powder obtained after drying was passed through a 200-mesh sieve, and the sieved powder was pressed into shape. The mold size was 24 mm × 7.6 mm, the pressing pressure was 300 MPa, and the pressure holding time was 1 min. Next, vacuum sintering was performed. The sintering temperature was 1450 °C, the temperature control accuracy was ±1 °C, and the maximum temperature holding time was 1 h. The degree of vacuum in the furnace was maintained at 10<sup>-3</sup>–10<sup>-2</sup> Pa during the sintering process. The sintered cermet samples were ground and polished with SiC water sand to obtain the polishing samples. As shown in Table 2, cermets with different Ta contents were successively denoted as cermet A, cermet B, cermet C, and cermet D.

The microstructure of (Ti,W)C-based cermets was observed by scanning electron microscopy (SEM, GeminiSEM300, Carl Zeiss AG, Oberkochen, Germany) and the grain size was measured by ImageJ software (ImageJ1.0, National Institutes of Health, Bethesda, MD, USA). The phase composition of cermet was characterized by X-ray diffraction (θ–2θ) with Cu-K<sub>α</sub> (40 kV and 40 mA) radiation and scanning rate of 4°/min (XRD, Empyrean, PANalytical, Malvern, UK). Measurement of relative density of cermets was determined by Archimedes' method. The hardness of the cermet was measured using the Vickers hardness tester (430SVD, Wolpert, OH, USA) under a load of 9.8 N for 15 s. The transverse breaking strength (TRS) was measured using the electronic universal material testing machine

(Instron 5967, Laizhou Keyi Test Instrument, Laizhou, China). The fracture toughness ( $K_{IC}$ ) of the cermet was measured using a single-edge notched bend (SENB) method. Immersion corrosion was studied in 0.5 mol/L  $HNO_3$  solution.

### 3. Results and Discussion

#### 3.1. Microstructure and Phase Composition of (Ti,W)C-Based Cermets

Figure 2 shows the XRD patterns of the (Ti,W)C-xTa-based cermets before and after vacuum sintering at 1450 °C for 1 h. The phase of the original powder after the mixed ball milling was (Ti,W)C, TiN, Ni,  $Mo_2C$ , and a small amount of WC. The diffraction peak of  $Mo_2C$  was detected instead of Mo, which is attributed to the solid solution of Mo and element C in the raw material used in the long ball milling process. The WC diffraction peak was assigned to shedding from the milling ball used in the ball milling process [19]. After sintering at 1450 °C for 1 h, the diffraction peaks of the  $Mo_2C$ , TiN, and WC disappeared from the XRD pattern; however, the diffraction peaks arising from the (Ti,W)C and Ni-based solid solution remained, while the other substances were dissolved during the sintering process [20]. It was observed from the local magnified XRD patterns in Figure 2b that all the diffraction peaks corresponding to (Ti,W)C after the sintering shifted to higher angles and the lattice constant decreased compared to those of the original powder before the sintering. The  $Mo_2C$ , TiN, and WC were dissolved-precipitated during the sintering process, and dissolved with (Ti,W)C to form a (Ti,W,Mo)C solid solution [21]. The atomic radius of Mo was smaller than those radii of Ti and W; therefore, with the formation of the (Ti,W,Mo)C solid solution, the lattice constant of (Ti,W)C decreased and the diffraction peak shifted.

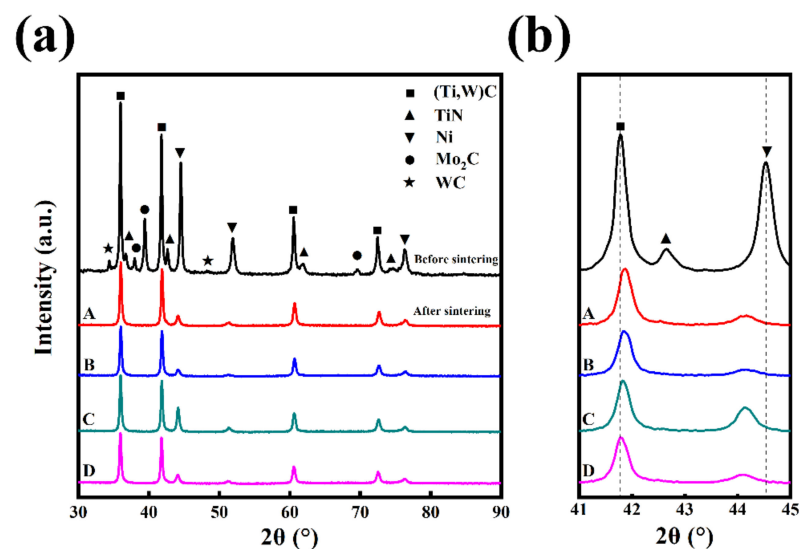


**Figure 2.** (a) XRD patterns of the (Ti,W)C-xTa-based cermets before and after sintering (before sintering: x = 3 wt.%), (b) Local magnification of (a).

However, with the increase in the Ta content of the (Ti,W)C-xTa-based cermets (Figure 2b patterns A~B), the diffraction peak corresponding to (Ti,W)C shifted into a lower angle and the lattice constant increased. This is because of the larger atomic radius of Ta than the radii of Ti and W. Ta diffused to form the (Ti,W,Ta)C solid solution during the sintering process. Further, the solid solution amount increased with the increase in the Ta content, and the offset increased accordingly [22]. All the diffraction peaks of the sintered Ni shifted to low angles, and the lattice constant increased. This result was mainly due to the formation of the solid solution of Mo and other elements in the binder phase during the sintering process. However, the intensity of the diffraction peak of the Ni-based solid solution increased with the addition of Ta, and the peak gradually shifted to a low angle, which might be due to the dissolution-precipitation behaviour of Ni as the metal binder phase during the sintering process. When the Ta content increased, the amount of

Ta dissolved by dissolution-precipitation also increased, and the lattice constant of the solid solution increased accordingly.

Figure 3 shows the SEM/BSE microstructures of the (Ti,W)C-xTa-based cermets with different Ta contents. As the Ta content changed from 0 wt.% to 3 wt.%, the microstructures were finer and more uniform, but when the Ta content increased to 5 wt.%, the microstructures' uniformity decreased. Figure 4 shows the average grain size and grain size distribution of the (Ti,W)C ceramic particles. The grain size of the ceramics first decreased and subsequently increased with the increase in the Ta content. When 3 wt.% Ta was added, the average grain size was the smallest, 0.803  $\mu\text{m}$ , and the grain size distribution was narrower. This change mainly depends on the presence of an appropriate amount of Ta, which can inhibit the dissolution-precipitation of Ti atoms and refine the grains in the structure. However, an excessive amount of Ta can cause agglomeration between the grains and form large particles [23–25].

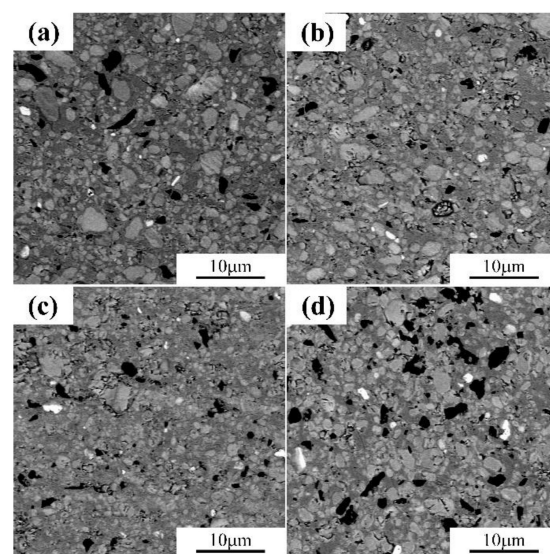


**Figure 3.** SEM/BSE images of (Ti,W)C-xTa-based cermets, x in wt.%: (a) x = 0, (b) x = 1, (c) x = 3, and (d) x = 5.

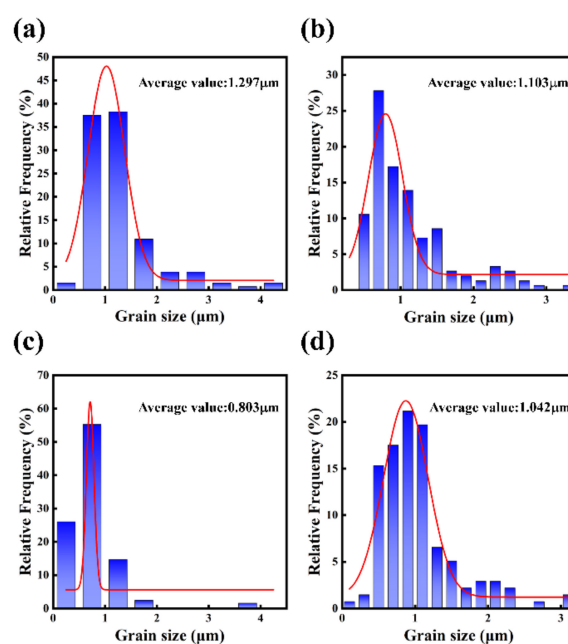


**Figure 4.** Grain size distributions of (Ti,W)C particles in the microstructures of (Ti,W)C-xTa-based cermets, x in wt.%: (a) x = 0, (b) x = 1, (c) x = 3, and (d) x = 5.

Figure 5 shows a high-magnification SEM image of the cermet C. The  $(\text{Ti,W})\text{C-xTa}$ -based cermets have a light gray core-gray rim structure (arrow A in Figure 5) and a white core-gray rim structure (arrow B in Figure 5), whereas the Ni binder phase is dark grey and continuously distributed in the matrix (as shown in Figure 5). In contrast to the traditional  $\text{Ti(C,N)}$ -based cermets, only a single-rim structure appeared in the  $(\text{Ti,W})\text{C}$ -based cermet; a double-layer annular structure (inner rim phase and outer rim phase) did not appear. Therefore, the cermet prepared using the  $(\text{Ti,W})\text{C}$  solid solution as the hard phase is beneficial for improving the interface effect in the material.

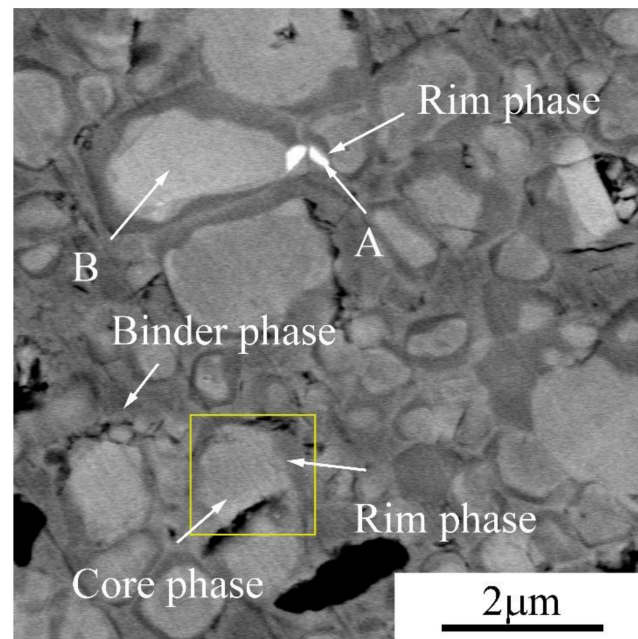
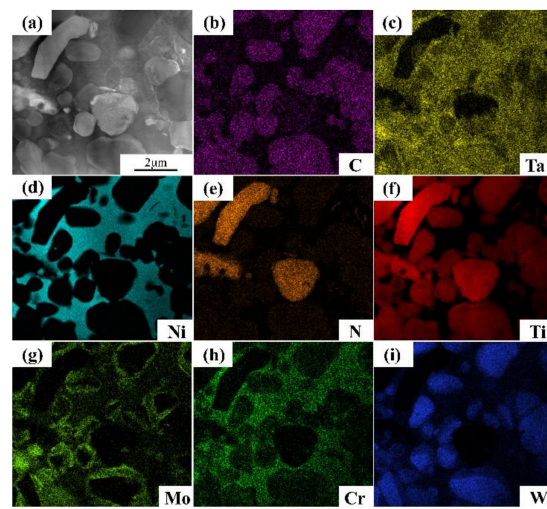


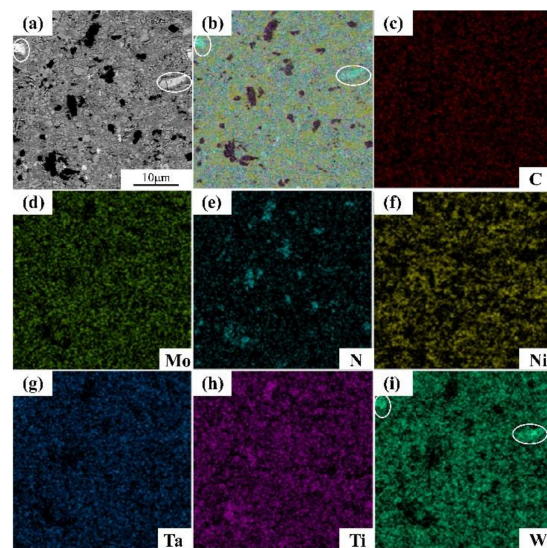
Figure 5. SEM image of the cermet C.

Figure 6 presents the STEM images and corresponding EDS results of the cermet C. There are obvious Ti and N enriched areas in the figure, which are  $\text{TiN}$  particles that were not completely dissolved during the sintering process. The light grey core phase was rich in Ti and W, the rim phase was rich in Mo, and the Ta element was uniformly distributed, which indicates that the core phase was mainly  $(\text{Ti, W, Ta})\text{C}$  particles, and the rim phase was mainly  $(\text{Ti, W, Ta, Mo})\text{C}$ . Figure 7 shows the SEM images and corresponding EDS results of the cermet C. From the EDS analysis, the distribution of each element was uniform, and W had an obvious enrichment area (the white circle of Figure 7a,b,i). Therefore, the white core phase is a W-rich  $(\text{Ti,W,Ta})\text{C}$  solid solution. Studies have shown that the W element in the W-rich  $(\text{Ti,W,Ta})\text{C}$  particles in  $(\text{Ti,W,Ta})\text{C}$ -based cermet comes from the grinding debris of the WC-Co ball grinding medium used in the ball milling process and not from the diffusion of W in the hard phase of  $(\text{Ti,W,Ta})\text{C}$  [26].

Figure 8 exhibits the fracture images of the four groups of the  $(\text{Ti,W})\text{C-xTa}$ -based cermets with different Ta contents. The fractures of the cermets all exhibit dimples and tearing edges formed by the fracture of the bonding phase and plastic deformation, the interface separation between two hard phase, and the fracture of the local large-grained hard phase along the cleavage plane. This indicates that cermet experienced brittle fractures and plastic fractures. From Figure 8 a, d, it is evident that there are pores and large particles in the fracture. The main reason for this is that Ta itself has a strong affinity toward C and N atoms; therefore, it preferentially attaches to the hard phase to strengthen the structure of the annular phase and refine the grain. However, the addition of excess Ta causes the grain in the cermet to grow abnormally and form pores in the material.



**Figure 6.** STEM image of the cermet C: (a) DF-STEM image, (b–i) EDS results corresponding to (a).



**Figure 7.** SEM image of the cermet C: (a) SEM image, (b–i) EDS results corresponding to (a).

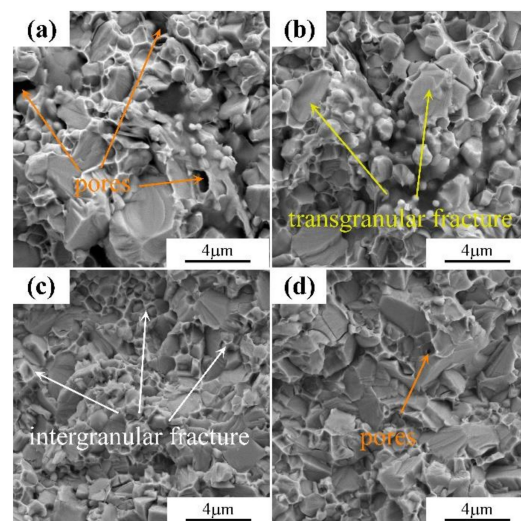


**Figure 8.** SEM micrographs of the fracture surface of the (Ti,W)C-xTa-based cermet, x in wt.%: (a) x = 0, (b) x = 1, (c) x = 3, and (d) x = 5.

### 3.2. Mechanical Properties

The relative density and mechanical properties of the (Ti,W)C-xTa-based cermets sintered at 1450 °C for 1 h are shown in Figure 9. The relative density of the (Ti,W)C-xTa-based cermet with different Ta contents increased and subsequently decreased with the increase in the Ta content. When the Ta content was 3 wt.%, the relative density reached the maximum value, indicating that Ta improved the wettability of the binder phase to the (Ti,W)C solid solution and completely densified the sintered sample. When the Ta content was 5 wt.%, the relative density of the cermet decreased because the excess Ta leads to the formation of pores during the sintering process of the cermet. Therefore, the density of the material was reduced, which was consistent with the effect of the Ta content on the relative density of the Ti(C,N)-based cermets. However, the overall relative density of the (Ti,W)C-xTa-based cermets was higher than that of the Ti(C,N)-based cermets [27].

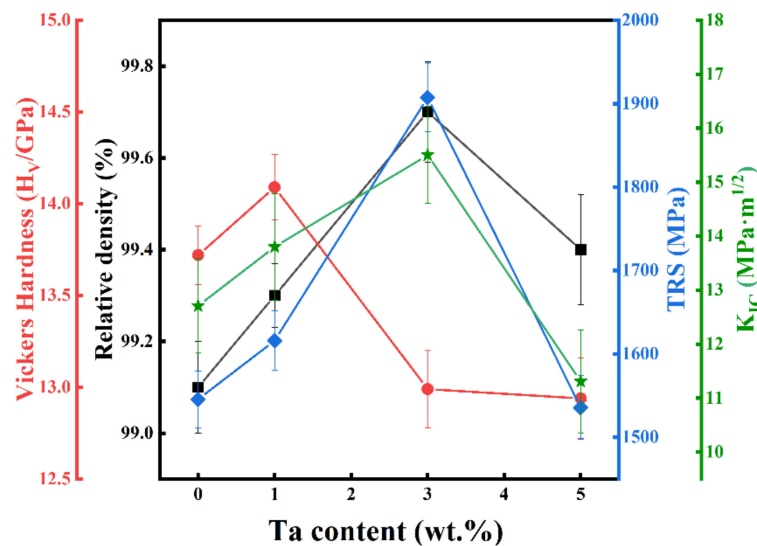


**Figure 9.** Effect of added Ta on the relative density and mechanical properties of the (Ti,W)C-xTa-based cermets.

When the Ta content increased from 0 to 5 wt.%, the hardness of the (Ti,W)C-xTa-based cermets increased first and subsequently decreased; it reached a maximum at 14.1 GPa when 1 wt.% Ta was added, as shown in Figure 9. Compared with the cermets without Ta, the increase in the hardness was small. When the Ta content was 3 wt.%, the hardness decreased significantly, which was lower than that of the samples without Ta. When the Ta content was increased to 5 wt.%, the hardness only decreased slightly. When a small amount of Ta was added, the hardness was improved mainly because the Ta promoted the refinement of the ceramic particles, and the Ta was evenly distributed in the cermet as the hard phase (as shown in Figure 6), which was conducive to the improvement in the hardness of materials. However, excess Ta would produce pores, lower the density of the material, and promote agglomeration between the particles, thus reducing the hardness of the material.

The influence of the Ta content on the TRS and fracture toughness of the (Ti,W)C-xTa-based cermets are shown in Figure 9. With the increase in the Ta content, the TRS and fracture toughness of the cermets first increased and subsequently decreased. Further, the TRS and fracture toughness reached the maximum values of 1907.5 MPa and 15.5  $\text{MPa}\cdot\text{m}^{1/2}$ , respectively, when the Ta content was 3 wt.%. The main reasons behind this phenomenon can be explained by considering the following factors: As evident from Figure 9, the relative density of the cermet reached the maximum value when 3 wt.% Ta was added. From the average grain size and grain size distribution of the (Ti,W)C ceramic particles, as shown in Figure 4, it was observed that the hard phase ceramic particles upon 3 wt.% Ta addition were small in size and were uniformly distributed. From the fracture morphology, as shown

in Figure 8, it was observed that the cermet with 3 wt.% Ta had more dimples and tear edges compared to the other components; therefore, its TRS and fracture toughness were higher than those of other components. When the Ta content reached 5 wt.%, the TRS and fracture toughness of the sample decreased sharply, obtaining values lower than those of the cermet without Ta. The reason for the decrease in the hardness is similar to that for the cermet with 5 wt.% Ta—the formation of pores and agglomeration of ceramic particles.

We systematically compared our experimental results with those in the literature, and the results are shown in Figure 10 [28–39]. It is evident from the figure that the (Ti,W)C-3Ta-30Ni cermet in this study exhibits excellent fracture toughness while obtaining good hardness. The problem of the low toughness of the cermet is greatly improved, and it is of great significance to the field of high-speed cutting tools.

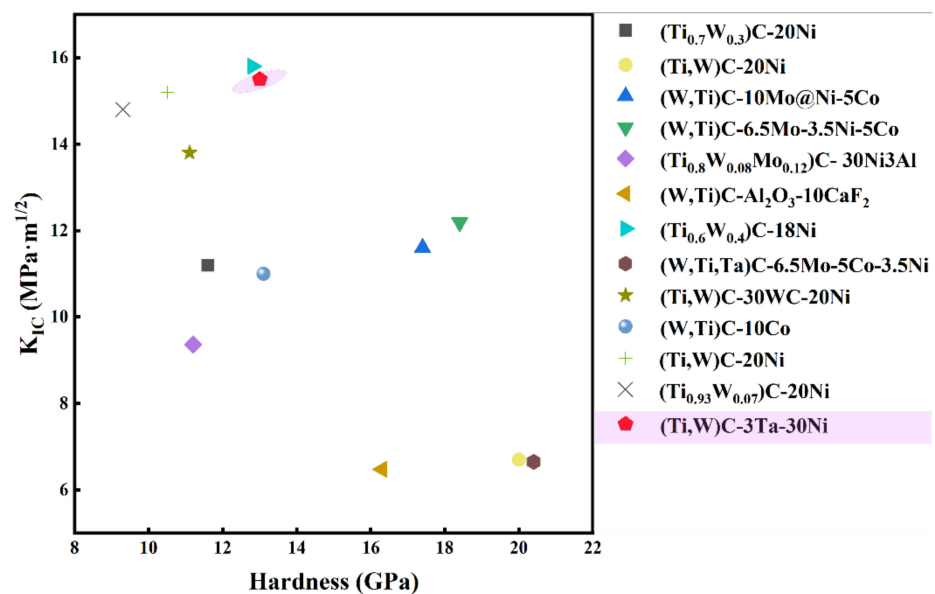
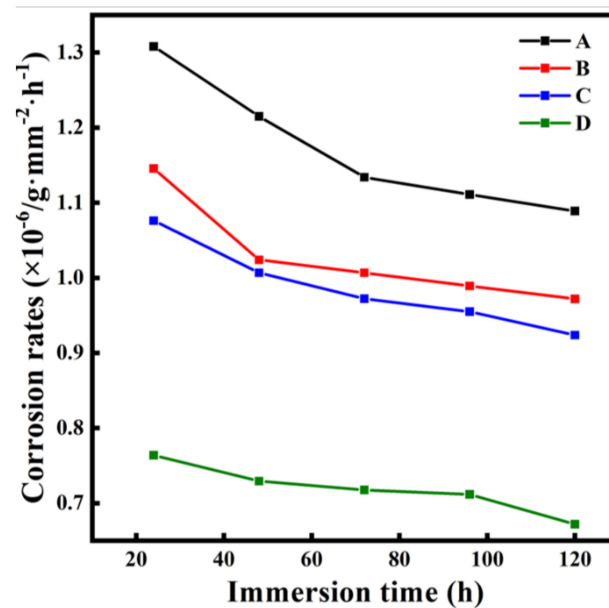


Figure 10. Comparison of (Ti,W)C-3Ta-30Ni cermet prepared in this work with other studies.

### 3.3. Immersion Corrosion

Figure 11 shows the corrosion rate curve of the (Ti,W)C-xTa-based cermets in 0.5 mol/L HNO<sub>3</sub> solution with a varying immersion time. It was observed that the corrosion rate curves of the four groups of the cermets with different Ta contents, A, B, C and D, showed the same trend with the increase in immersion time: the corrosion rates gradually decreased with time and the change was stable. The initial corrosion rate was relatively high mainly because the large clean surface of the sample surface was exposed to the corrosive solution after the polishing treatment, and the binder phase was corroded first. After the binder phase on the surface of the cermet was corroded, the corrosive liquid corroded the internal binder phase of the cermet through the surface holes. Owing to the high density of the cermet, it was difficult for the corrosive liquid to penetrate the cermet; therefore, the corrosion degree of the internal binder phase dropped, and the overall corrosion rate decreased accordingly. With the increase in the Ta content, the corrosion rate of the (Ti,W)C-xTa-based cermets decreased. When the Ta content exceeds 3 wt.%, the corrosion rate of the cermet decreases greatly. As the corrosion time increases, the corrosion rate decreases steadily.

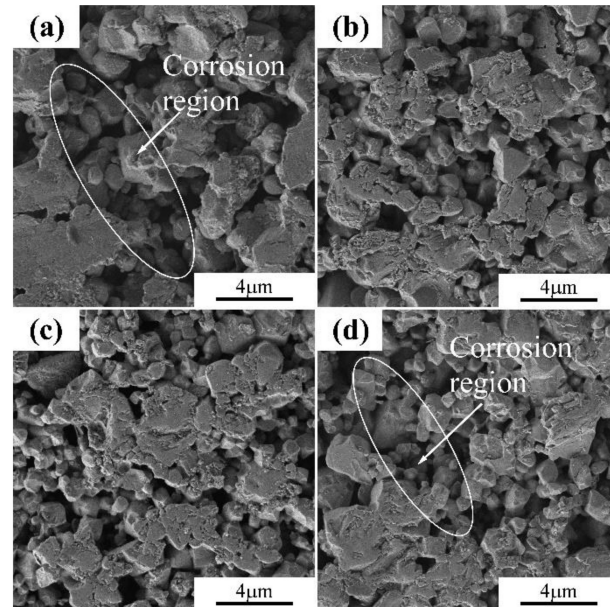


**Figure 11.** Corrosion rates of the cermet with different Ta contents as a function of time in 0.5 mol/L  $\text{HNO}_3$  solution, A-0 wt.% Ta, B-1 wt.% Ta, C-3 wt.% Ta, and D-5 wt.% Ta.

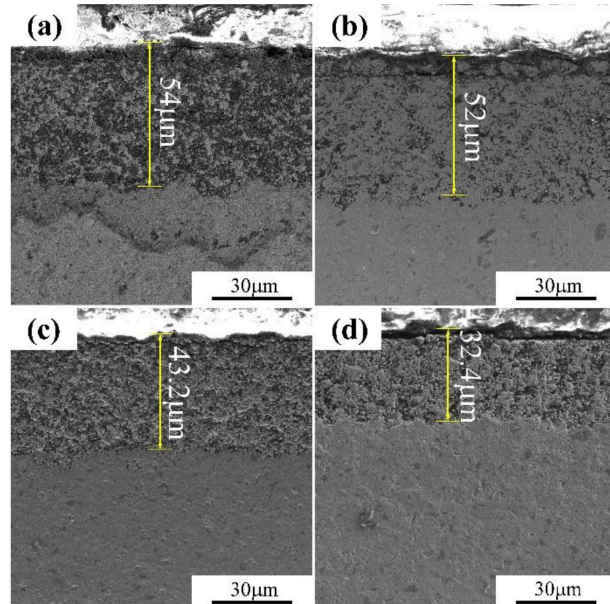
Figure 12 shows the SEM images of the (Ti,W)C-xTa-based cermet after corrosion. The surface morphologies of the cermet with different Ta contents were corroded to different extents. In the case of the A-component cermet without Ta impurities, the corrosion degree and corrosion depth of the surface binder phase were clear. They were higher than those for the other three groups of the cermet containing Ta. Further, with the increase in the Ta content, the number of surface corrosion pits gradually decreased, indicating that the corrosion resistance of the cermet was improved. According to Yi et al. [40], the corrosion behaviour of cermet in a nitric acid solution was mainly manifested by the dissolution of the binder phase in the corrosive solution and the oxidation of carbide in the hard phase in the oxidising corrosive solution. The corrosion of the cermet was primarily determined by the synergistic effect of the hard phase and binder phase. The hard phase was a brittle ceramic material that was prone to brittle fracture, whereas the binder phase was prone to plastic deformation, extrusion fall-off, and other forms of failure. The uniformity of the microstructure, the strength, and the toughness of cermet have a certain influence on the corrosion resistance of materials. Further, the solid solution strengthening of the secondary carbides in the binder phase exerts a certain influence on the corrosion resistance of the cermet [29].

Figure 13 depicts the cross-sectional morphology of the (Ti,W)C-xTa-based cermet after corrosion. After the immersion of the cermet with different Ta contents in 0.5 mol/L  $\text{HNO}_3$  solution for 120 h, the corrosion depth gradually decreased with the increase in the Ta content, from 54 to 32.4  $\mu\text{m}$ , indicating that the addition of Ta enhanced the corrosion resistance of the materials in the acidic solution. Further, a split layer at the upper end of the corrosion region of the sample was observed, as shown in the figure. The cross-section was investigated through an energy spectrum analysis; taking the cermet C as an example, the results are shown in Figure 14. The presence of a large amount of Ta and O was detected in the outermost split layer of the cermet, indicating that a Ta-rich oxide layer was formed on the surface of the cermet. During the corrosion process of the material in the  $\text{HNO}_3$  solution, the oxide layer has an obvious tendency to peel off. In the EDS analysis of the corroded cermet section, it is evident that there is almost no nickel in the entire corroded area, indicating that nickel will be preferentially corroded during the corrosion process, and will peel off from the ceramic particles to form a large number of corrosion pits. The corrosion of the binder phase is the main failure mode when the cermet is eroded [41]. With the increase in the Ta content in the cermet, the uniformity and hardness of the cermet can

improve its corrosion resistance. Additionally, the greater the content of Ta in the solid solution of the binder phase, the stronger the corrosion resistance of the binder phase, and the smaller the corrosion depth of the cermet [42].



**Figure 12.** SEM images of the corrosion surface of the (Ti,W)C-xTa-based cermets immersed in 0.5 mol/L HNO<sub>3</sub> solution for 120 h, x in wt.%: (a) x = 0, (b) x = 1, (c) x = 3, and (d) x = 5.



**Figure 13.** SEM images of the corrosion cross-sectional area of the (Ti,W)C-xTa-based cermets immersed in 0.5 mol/L HNO<sub>3</sub> solution for 120 h, x in wt.%: (a) x = 0, (b) x = 1, (c) x = 3, and (d) x = 5.

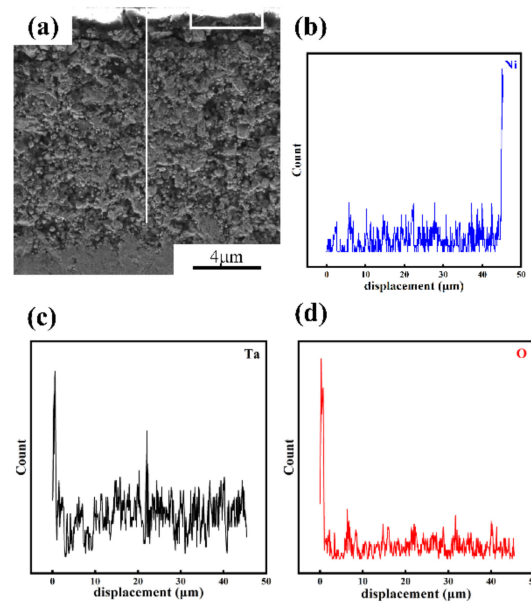


**Figure 14.** Corrosion fracture image of the cermet C: (a) SEM image; (b–d) corresponding EDS results.

#### 4. Conclusions

The microstructure, mechanical properties, and corrosion resistance of the (Ti,W)C-xTa-based cermets with different Ta contents were studied. The conclusions of this study are as follows:

(1) The microstructure of all the (Ti,W)C-xTa-based cermets have a light gray core-gray rim structure and a white core-gray rim structure. With the addition of Ta, the light grey core was transformed into a (Ti,W,Ta)C solid solution, and the white core phase was a W-rich (Ti,W,Ta)C solid solution.

(2) When the Ta content was in the range of 0–3 wt.%, with the increase in the Ta content, the microstructure distribution became uniform, and the grain size gradually decreased. As the Ta content continued to increase, the uniformity of the microstructure distribution worsened, the particles appeared agglomerated, and large grains were formed. When the Ta content was 1 wt.%, the hardness reached the maximum value of 14.1 GPa. In addition, the flexural strength and fracture toughness reached the maximum values of 1907.5 MPa and 15.5 MPa·m<sup>1/2</sup>, respectively, when the Ta content was 3 wt.%. When the Ta content exceeded 3 wt.%, the mechanical properties of the cermets noticeably decreased.

(3) The addition of Ta can significantly improve the corrosion resistance of the (Ti,W)C-xTa-based cermets. Further, with the increase in the Ta content, the corrosion resistance of the material in the HNO<sub>3</sub> solution improved. The corrosion rate of the (Ti,W)C-xTa-based cermets decreased gradually with the increase in the immersion time and Ta content. The corrosion rate of the (Ti,W)C-xTa-based cermets decreased with the increase in the Ta content, and the change was stable with time. The corrosion behaviour of the material in the HNO<sub>3</sub> solution is attributed to the dissolution of the surface-Ni-based solid solution and the peeling behaviour of the oxide layer formed on the surface.

**Author Contributions:** Conceptualization, R.T., S.Z. and T.G.; methodology, J.L.; software, B.J.; validation, M.Y.; formal analysis, S.Z. and J.L.; investigation, M.Y.; data curation, S.Z.; writing—original draft preparation, J.L. and Q.L.; writing—review and editing, Q.L. All authors have read and agreed to the published version of the manuscript.

**Funding:** This work was supported by the Guangdong Major Project of Basic and Applied Basic Research (2021B0301030001); Key-Area Research and Development Program of Guangdong Province (2021B0707050001, 2019B121204001, and 2020B010181001); the Chaozhou Science and Technology Project (2019PT01); the Self-innovation Research Funding Project of Hanjiang Laboratory (HJL202012A001, HJL202012A002, and HJL202012A003); and the Major Science and Technology Project in Zhongshan City, Guangdong Province (2019AG029). This work was also supported by the

Joint Fund of the Ministry of Education for Pre-research of Equipment (6141A02022257), the Science Challenge Project (TZ2016001), the National Natural Science Foundation of China (51861145306, 51872212, and 51972244), and the 111 Project (B13035). It was also supported by the International Science and Technology Cooperation Program of China (2018YFE0103600) and the Technological Innovation of Hubei Province, China (2019AAA030).

**Institutional Review Board Statement:** Not applicable.

**Informed Consent Statement:** Not applicable.

**Data Availability Statement:** The raw and processed data required to reproduce these results are available by contacting the authors.

**Conflicts of Interest:** The authors declare no conflict of interest.

## References

1. Genga, R.M.; Akdogan, G.; Westraadt, J.E.; Cornish, L.A. Microstructure and Material Properties of PECS Manufactured WC-NbC-CO and WC-TiC-Ni Cemented Carbides. *Int. J. Refract. Met. Hard Mater.* **2015**, *49*, 240–248. [\[CrossRef\]](#)
2. Zhou, M.; Yang, H.; Zhang, H.; Zhang, J.; Xia, X.; Liu, X. The Research on Cutting Performance of Two Kinds of Ti(C, N)-Based Cermet Cutters. *Key Eng. Mater.* **2014**, *589–590*, 332–336. [\[CrossRef\]](#)
3. Yun, H.; Zou, B.; Wang, J. Effects of Sintering Temperature and Nano Ti(C,N) on the Microstructure and Mechanical Properties of Ti(C,N) Cermets Cutting Tool Materials with Low Ni-Co. *Mater. Sci. Eng. A* **2017**, *705*, 98–104. [\[CrossRef\]](#)
4. Xu, Q.; Zhao, J.; Ai, X. Fabrication and Cutting Performance of Ti(C,N)-Based Cermet Tools Used for Machining of High-Strength Steels. *Ceram. Int.* **2017**, *43*, 6286–6294. [\[CrossRef\]](#)
5. Córdoba, J.M.; Chicardi, E.; Gotor, F.J. Liquid-Phase Sintering of Ti(C,N)-Based Cermets. the Effects of Binder Nature and Content on the Solubility and Wettability of Hard Ceramic Phases. *J. Alloys Compd.* **2013**, *559*, 34–38. [\[CrossRef\]](#)
6. Menezes, P.L.; Ingle, S.P.; Nosonovsky, M.; Kailas, S.V.; Lovell, M.R. *Tribology for Scientists and Engineers: From Basics to Advanced Concepts*; Springer: Cham, Switzerland, 2013; Volume 9781461419, pp. 1–948.
7. Yu, H.; Liu, W.; Zheng, Y. Microstructure and Mechanical Properties of Liquid Phase Sintered Mo<sub>2</sub>FeB<sub>2</sub> Based Cermets. *Mater. Des.* **2011**, *32*, 3521–3525. [\[CrossRef\]](#)
8. Kwon, W.T.; Park, J.S.; Kang, S. Effect of Group IV Elements on the Cutting Characteristics of Ti(C,N) Cermet Tools and Reliability Analysis. *J. Mater. Process. Technol.* **2005**, *166*, 9–14. [\[CrossRef\]](#)
9. Xiong, H.; Wu, Y.; Li, Z.; Gan, X.; Zhou, K.; Chai, L. Comparison of Ti(C, N)-Based Cermets by Vacuum and Gas-Pressure Sintering: Microstructure and Mechanical Properties. *Ceram. Int.* **2018**, *44*, 805–813. [\[CrossRef\]](#)
10. Rubiano Buitrago, J.D.; Gil Plazas, A.F.; Herrera Quintero, L.K. Influence of TiC and Cr<sub>3</sub>C<sub>2</sub> Additions on the Mechanical Properties of a (W-Ti-Cr)-Co Sintered Hardmetal. *J. Mater. Res. Technol.* **2019**, *8*, 5736–5744. [\[CrossRef\]](#)
11. Nie, R.; Peng, Y.; Liu, G.; Yan, W.; Yan, L.; Zhou, W.; Zhou, S.; Zhang, W.; Jin, P. Microstructure and Properties of Ti(C, N)-Based Cermet with Multi-Core-Rim Microstructure: Effect of (Ti, W, Ta) (C, N) Pre-Solid Solution Composition. *J. Mater. Sci.* **2022**, *57*, 4583–4593. [\[CrossRef\]](#)
12. Huang, S.G.; Liu, C.; Liu, B.L.; Vleugels, J.; Huang, J.H.; Lauwers, B.; Qian, J.; Mohrbacher, H. Microstructure and Mechanical Properties of (Nb,W,Ti)(C,N)-Ni Solid Solution Cermets with 6 to 20 Wt% Ni. *Int. J. Refract. Met. Hard Mater.* **2022**, *103*, 105757. [\[CrossRef\]](#)
13. Wang, G.D. *Production Principle of Cemented Carbide*, 1st ed.; Metallurgical Industry Press: Beijing, China, 1988.
14. Lin, Z.; Xiong, J.; Guo, Z.; Zhou, W.; Wan, W.; Yang, L. Effect of Mo<sub>2</sub>C Addition on the Microstructure and Fracture Behavior of (W,Ti)C-Based Cemented Carbides. *Ceram. Int.* **2014**, *40*, 16421–16428. [\[CrossRef\]](#)
15. Zhang, H.; Yan, J.; Zhang, X.; Tang, S. Properties of Titanium Carbonitride Matrix Cermets. *Int. J. Refract. Met. Hard Mater.* **2006**, *24*, 236–239. [\[CrossRef\]](#)
16. Han, C.; Kong, M. Fabrication and Properties of TiC-Based Cermet with Intra/Intergranular Microstructure. *Mater. Des.* **2009**, *30*, 1205–1208. [\[CrossRef\]](#)
17. Manoj Kumar, B.V.; Balasubramaniam, R.; Basu, B. Electrochemical Behavior of TiCN-Ni-Based Cermets. *J. Am. Ceram. Soc.* **2007**, *90*, 205–210. [\[CrossRef\]](#)
18. Naidoo, M.; Johnson, O.; Sigalas, I.; Herrmann, M. Influence of Tantalum on the Microstructure and Properties of Ti(C,N)-Ni Cermets. *Int. J. Refract. Met. Hard Mater.* **2014**, *42*, 97–102. [\[CrossRef\]](#)
19. Park, S.; Kang, Y.J.; Kwon, H.J.; Kang, S. Synthesis of (Ti, M1, M2)(CN)-Ni Nanocrystalline Powders. *Int. J. Refract. Met. Hard Mater.* **2006**, *24*, 115–121. [\[CrossRef\]](#)
20. Han, C.; Tian, C. Effect of Mo<sub>2</sub>C on the Microstructure and Mechanical Properties of (Ti, W)C-Ni Cermets. *Powder Metall. Met. Ceram.* **2014**, *53*, 57–63. [\[CrossRef\]](#)
21. Zhang, G.; Xiong, W.; Yang, Q.; Yao, Z.; Chen, S.; Chen, X. Effect of Mo Addition on Microstructure and Mechanical Properties of (Ti,W)C Solid Solution Based Cermets. *Int. J. Refract. Met. Hard Mater.* **2014**, *43*, 77–82. [\[CrossRef\]](#)
22. Naidoo, M.; Johnson, O.; Sigalas, I.; Herrmann, M. Preparation of Ti-Ta-(C,N) by Mechanical Alloying Ti(C,N) and TaC. *Int. J. Refract. Met. Hard Mater.* **2013**, *37*, 67–72. [\[CrossRef\]](#)

23. Yang, T.; Shi, K.; Liu, X.; Sang, J.; Xia, X.; Su, W.; Ren, J.; Zhang, R.; Xing, B. Structure Formation and Properties of WC-(W,Ti)C-Ti(C,N)-TaC-Co Gradient Cemented Carbides with Cubic Phases Free in the Surface Layer. *Int. J. Refract. Met. Hard Mater.* **2021**, *98*, 105548. [[CrossRef](#)]
24. Liu, C.; Lin, N.; He, Y.H. Influence of Mo<sub>2</sub>C and TaC Additions on the Microstructure and Mechanical Properties of Ti(C,N)-Based Cermets. *Ceram. Int.* **2016**, *42*, 3569–3574. [[CrossRef](#)]
25. Wu, P.; Zheng, Y.; Zhao, Y.; Yu, H. Effect of TaC Addition on the Microstructures and Mechanical Properties of Ti(C,N)-Based Cermets. *Mater. Des.* **2010**, *31*, 3537–3541. [[CrossRef](#)]
26. Chen, X.; Xiong, W.; Qu, J.; Yang, Q.; Yao, Z.; Huang, Y. Microstructure and Mechanical Properties of (Ti,W,Ta)C-XMo-Ni Cermets. *Int. J. Refract. Met. Hard Mater.* **2012**, *31*, 56–61. [[CrossRef](#)]
27. Hu, H.; Cheng, Y.; Yin, Z.; Zhang, Y.; Lu, T. Mechanical Properties and Microstructure of Ti(C, N) Based Cermet Cutting Tool Materials Fabricated by Microwave Sintering. *Ceram. Int.* **2015**, *41*, 15017–15023. [[CrossRef](#)]
28. Seo, M.; Kim, J.; Kang, S. Effect of Carbon Content on the Microstructure and Properties of (Ti 0.7W0.3)C-Ni Cermet. *Int. J. Refract. Met. Hard Mater.* **2011**, *29*, 424–428. [[CrossRef](#)]
29. Peng, J.; Yi, M.; Xiao, G.; Chen, Z.; Zhang, J.; Chen, H.; Xu, C. Low-Temperature and Ultrafast Dual-Powder Spark Plasma Sintering of (W,Ti)C Cermets with the Addition of Metal Core-Shell Nanopowder. *Int. J. Refract. Met. Hard Mater.* **2022**, *107*, 105901. [[CrossRef](#)]
30. Wang, Z.; Wang, J.; Xu, Y.; Yi, M.; Xiao, G.; Chen, Z.; Zhang, J.; Chen, H.; Xu, C. Microstructure and Mechanical Properties of (Ti,W)C Cermets Prepared by Ultrafast Spark Plasma Sintering. *Ceram. Int.* **2022**, *48*, 15613–15621. [[CrossRef](#)]
31. Huang, B.; Xiong, W.; Zhang, M.; Jing, Y.; Li, B.; Luo, H.; Wang, S. Effect of W Content in Solid Solution on Properties and Microstructure of (Ti,W)C-Ni<sub>3</sub>Al Cermets. *J. Alloys Compd.* **2016**, *676*, 142–149. [[CrossRef](#)]
32. Wang, J.; Yi, M.; Xu, C.; Xiao, G.; Chen, Z.; Zhang, J.; Wang, L. Mechanical Property and Cutting Performance of (W,Ti)C Based Ceramic Composites with the Addition of Nano-Sized CaF<sub>2</sub>. *Int. J. Refract. Met. Hard Mater.* **2021**, *99*, 105607. [[CrossRef](#)]
33. Xiong, H.; Wen, Y.; Li, Z.; Zhou, K. Dual-Grained (Ti, W)C-Ni Cermets by Two-Step Carbonization: Hot Isotropic Press Sintering of NiTiW Alloys and Colloidal Graphite. *J. Am. Ceram. Soc.* **2019**, *102*, 4296–4305. [[CrossRef](#)]
34. Zhang, Z.; Xu, Y.; Yi, M.; Jiang, S.; Chen, Z.; Xiao, G.; Zhang, J.; Chen, H.; Xu, C. Synthesis and Characterization of Extremely Hard and Strong (W,Ti,Ta)C Cermet by Spark Plasma Sintering. *Int. J. Refract. Met. Hard Mater.* **2022**, *105*, 105831. [[CrossRef](#)]
35. Park, S.; Kang, S. Toughened Ultra-Fine (Ti,W)(CN)-Ni Cermets. *Scr. Mater.* **2005**, *52*, 129–133. [[CrossRef](#)]
36. Wu, Y.; Xin, H.X.; Zhai, Y.C. Effect of Ta, Nb and V Additions on the Microstructure and Mechanical Properties of (W,Ti)C-Co. *Adv. Mater. Res.* **2012**, *535–537*, 783–786. [[CrossRef](#)]
37. Kwon, H.; Suh, C.Y.; Kim, W. Microstructure and Mechanical Properties of (Ti,W)C-Ni Cermet Prepared Using a Nano-Sized TiC-WC Powder Mixture. *J. Alloys Compd.* **2015**, *639*, 21–26. [[CrossRef](#)]
38. Rafiaei, S.M.; Kim, J.H.; Kang, S. Effect of Nitrogen and Secondary Carbide on the Microstructure and Properties of (Ti<sub>0.93</sub>W<sub>0.07</sub>)C-Ni Cermets. *Int. J. Refract. Met. Hard Mater.* **2014**, *44*, 123–128. [[CrossRef](#)]
39. Xiong, Y.; Kim, M.; Seo, O.; Schoenung, J.M.; Kang, S. (Ti,W)C-Ni Cermets by Laser Engineered Net Shaping. *Powder Metall.* **2010**, *53*, 41–46. [[CrossRef](#)]
40. Yi, C.; Fan, H.; Xiong, J.; Guo, Z.; Dong, G.; Wan, W.; Chen, H. Effect of WC Content on the Microstructures and Corrosion Behavior of Ti(C,N)-Based Cermets. *Ceram. Int.* **2013**, *39*, 503–509. [[CrossRef](#)]
41. Wan, W.; Xiong, J.; Liang, M. Effects of Secondary Carbides on the Microstructure, Mechanical Properties and Erosive Wear of Ti(C,N)-Based Cermets. *Ceram. Int.* **2017**, *43*, 944–952. [[CrossRef](#)]
42. Wan, W.; Xiong, J.; Guo, Z.; Dong, G.; Yi, C. Effects of Cr<sub>3</sub>C<sub>2</sub> Addition on the Erosion-Corrosion Resistance of Ti(C,N)-Based Cermets in Alkaline Conditions. *Tribol. Int.* **2013**, *64*, 178–186. [[CrossRef](#)]